Landscape Ecol (2020) 35:859–878
https://doi.org/10.1007/s10980-020-00983-0

RESEARCH ARTICLE

Burn weather and three-dimensional fuel structure determine post-fire tree mortality

Sean M. A. Jeronimo · James A. Lutz · Van R. Kane · Andrew J. Larson · Jerry F. Franklin

Received: 12 March 2019 / Accepted: 5 February 2020 / Published online: 20 February 2020

Abstract

Context Post-fire tree mortality is a spatially structured process driven by interacting factors across multiple scales. However, empirical models of fire-caused tree mortality are generally not spatially explicit, do not differentiate among scales, and do not differentiate immediate from delayed mortality.

Objectives We aimed to quantify cross-scale linkages between forest structure—including spatial patterns of trees—and the progression of mortality 1–4 years post-fire in terms of rates, causes, and underlying demography.

Methods We used data from a long-term study site in the Sierra Nevada, California to build a post-fire tree mortality model predicted by lidar-measured estimates of structure. We calculated structural metrics at scales from individual trees to 90 × 90 m neighborhoods and combined them with metrics for topography, site water balance, and burn weather to predict immediate and delayed post-fire tree mortality.

Results Mortality rates decreased while average diameter of newly killed trees increased each year post-fire. Burn weather predictors as well as interactive terms across scales improved model fit and parsimony. Including landscape-scale information improved finer-scale predictions but not vice versa. The amount of fuel, fuel configuration, and burning conditions predicted total mortality at broader scales while tree group-scale fuel connectivity, tree species fire tolerance, and local stresses predicted the fine-scale distribution, timing, and agents of mortality.

Conclusions Landscape-scale conditions provide the template upon which finer-scale variation in post-fire tree mortality is arranged. Post-fire forest structure is associated with the etiologies of different mortality agents, and so landscape-level heterogeneity is a key part of ecosystem stability and resilience.

Keywords Post-fire tree mortality · Spatial patterns · Cross-scale interactions · Delayed mortality · Mortality agents · Sierra nevada mixed-conifer · Smithsonian ForestGEO · Yosemite forest dynamics plot

Electronic supplementary material The online version of this article (https://doi.org/10.1007/s10980-020-00983-0) contains supplementary material, which is available to authorized users.

S. M. A. Jeronimo (✉) · V. R. Kane · J. F. Franklin
School of Environmental and Forest Sciences, College of the Environment, University of Washington, Box 352100, Seattle, WA 98195, USA
e-mail: jeronimo@uw.edu

J. A. Lutz
Wildland Resources Department, Quinney College of Natural Resources, Utah State University, 5230 Old Main Hill, Logan, UT 84322, USA

A. J. Larson
W.A. Franke College of Forestry and Conservation, University of Montana, 32 Campus Drive, Missoula, MT 59802, USA

Introduction

Post-fire tree mortality varies with pre-fire forest structure (Stephens and Moghaddas 2005; Lydersen et al. 2017; Furniss et al. 2019; Kane et al. 2019). Since tree mortality changes forest structure, this represents a pattern-process feedback between structure and tree population dynamics. This feedback is an important mechanism of ecosystem stability and resilience at multiple scales for fire-dependent forests (Larson and Churchill 2012; Parks et al. 2015).

Patterns of forest structure and post-fire tree mortality emerge in the context of a hierarchy of nested spatial scales (Kotliar and Wiens 1990; Palik et al. 2000; Boyden et al. 2012; Hessburg et al. 2015). Damage caused by fire and its effects on tree mortality vary depending on characteristics of individual trees, but also on vertical and horizontal spatial patterns at the scales of tree clumps and larger neighborhoods (Agee and Skinner 2005; Hessburg et al. 2005; Kennedy and Johnson 2014; Belote et al. 2015; Clyatt et al. 2016). For example, fire-caused mortality at the individual tree scale is broadly due to excessive radiative flux damaging crown and stem tissues (Smith et al. 2016), which occurs in accordance with individual tree characteristics like bark thickness and crown structure (Hood et al. 2018). Vertically continuous tree crowns can carry surface fires into the canopy (Stephens 1998; Agee and Skinner 2005) while horizontal patterns of trees can modify the way fire moves through a stand or across a landscape (Parsons et al. 2017, 2018). Heterogeneous patterns, such as closely-spaced aggregates of trees and canopy openings larger than the average mature tree crown, result in complex wind and convection fields. These factors induce varied and aggregated fire effects such as small-group torching, survival of dense regeneration patches with little or no surface fuels, and survival in topographically protected areas (Fulé and Covington 1998; Stephens and Fry 2005; Kolden et al. 2012; Parsons et al. 2017; Meddens et al. 2018). Dynamics at these scales act to maintain and enhance pre-fire clump and opening patterns (Kane et al. 2013, 2014). Pattern-process linkages like these also interact across hierarchical scales (Kotliar and Wiens 1990; Parsons et al. 2016).

Delayed post-fire tree mortality can also be affected by structure and spatial patterns at multiple scales. Delayed mortality, which can represent over 40% of total fire mortality, occurs following fires of all severities and usually takes place within 4–5 years after fire (Youngblood et al. 2009; Fettig et al. 2010; Hood et al. 2010; Van Mantgem et al. 2011; Prichard and Kennedy 2012; Miller et al. 2016). Delayed mortality can occur after nonlethal fire-caused damage to a tree's cambium and/or crown initiates a death spiral, ultimately killing the tree some years later. Common proximate agents of delayed mortality are carbon starvation, hydraulic failure, decay, bark beetles, wind, competition, or some combination of these (Filip et al. 2007; Smith et al. 2016). Many delayed mortality agents (e.g., insects, pathogens, and competition) are density-dependent. High stand density can additionally predispose trees to compounding stressors such as drought and bark beetles (Guarín and Taylor 2005; Hood and Bentz 2007; Das et al. 2008; Stephens et al. 2018). Like immediate mortality, delayed morality is the result of processes acting and interacting across scales. For example, regional drought can interact with fine-scale patterns of tree density and demography to drive bark beetle mortality (Guarín and Taylor 2005).

Our objective was to investigate how forest structure, spatial pattern, and cross-scale interactions influence immediate and delayed post-fire tree mortality at the scales of tree groups and neighborhoods. We sought to quantify these effects to improve the ecological understanding of pattern-process linkages related to post-fire tree mortality and to inform modeling options for use by forest managers. Our specific research questions were:

(1) How does tree mortality progress 1–4 years post-fire in terms of mortality rates and demographics?
(2) What elements of vertical forest structure and horizontal pattern predict immediate and delayed post-fire tree mortality at scales from small groups of trees to larger neighborhood patches?
(3) Are there interactions between effects at different scales, and are those interactions directional (i.e., broader to finer scales or finer to broader scales)?
(4) How does the prevalence of different mortality agents vary with changes in fine-scale predictors of post-fire tree mortality?

Methods

Study area

We studied tree mortality after the 2013 Rim Fire within Yosemite National Park, California (Fig. 1). The Rim Fire started on August 17, 2013 and burned 104,131 ha—including 31,519 ha in Yosemite National Park—and was declared out on October 23, 2013. Although fire effects on the adjacent Stanislaus National Forest included very large high-severity patches that burned under extreme weather conditions (Lydersen et al. 2014), effects in Yosemite were more mixed and provide an excellent opportunity to study the multi-scale effects of structure and pattern on tree mortality (Kane et al. 2015a; Blomdahl et al. 2019).

One complication of using the Rim Fire to study tree mortality is that it occurred in the midst of a multi-year drought (Lydersen et al. 2014). The drought may have exacerbated the post-fire stresses caused by fire damage and possibly resulted in higher mortality rates than would have been observed without a drought (van Mantgem et al. 2013, 2018). However, the 2013–2015 drought was similar to projected climate conditions for the 2050s (Cayan et al. 2008), and so results from this study should be directly relevant to understanding the forest dynamics of the near future.

We used post-fire tree mortality data from the Yosemite Forest Dynamics Plot (YFDP; Lutz et al. 2012), a 25.6 ha stem mapped plot affiliated with the Smithsonian ForestGEO network (Anderson-Teixeira et al. 2015; Lutz 2015; Lutz et al. 2018a). The YFDP is an old-growth sugar pine-white fir (*Pinus lambertiana–Abies concolor*) forest ranging from 1774 to 1911 m in elevation. The YFDP was established in 2009–2010 and a census of all woody stems $\geq$ 1 cm dbh has been conducted to determine recruitment and mortality each year since 2011.

The climate of the area is Mediterranean with cool moist winters and warm dry summers. Thirty-year

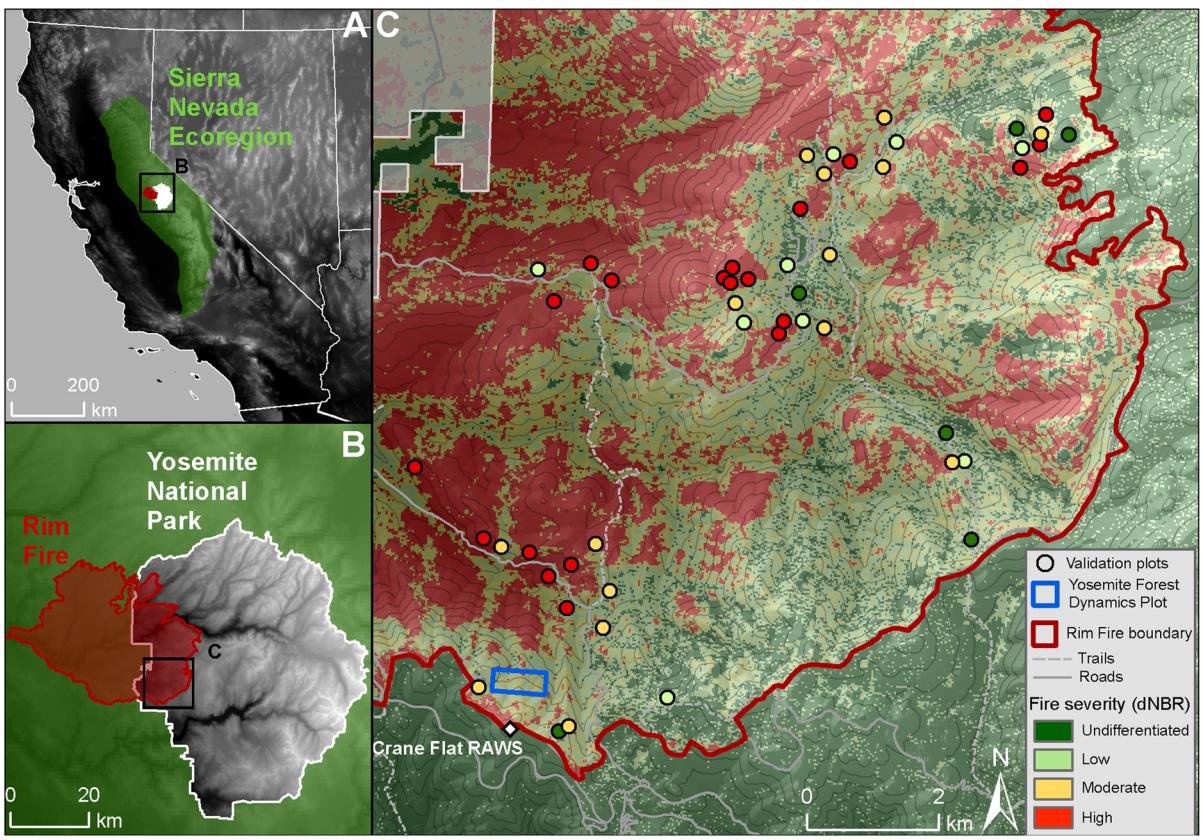

Fig. 1 Map of study area showing the Yosemite Forest Dynamics Plot, Crane Flat Weather Station, Rim Fire severity, the 2010 lidar acquisition, and validation plot locations. Validation plots are colored by satellite-derived fire severity class

climate normal temperatures range from a February minimum of − 3 °C to a July maximum of 26 °C. Winters are moderately snowy with snow accumulating into a springtime snowpack depth of approximately 1 m. Summers consistently include several months lacking precipitation.

Before the Rim Fire, the YFDP experienced a period of fire suppression starting in 1900, which interrupted a previously frequent fire regime (29.5 year point fire return interval) (Barth et al. 2015). Contemporary pre-fire forest conditions on the YFDP were representative of the fire-suppressed Sierra Nevada mixed-conifer zone at large, with high density and basal area (535.9 trees ha^{-1} and 64 m^2 ha^{-1} in 2010 vs. 84.9 trees ha^{-1} and 24.1 m^2 ha^{-1} in 1900) accompanied by a compositional shift from dominance by shade-intolerant species to shade-tolerant species (74% sugar pine and 20% white fir in 1900 vs. 45% sugar pine and 46% white fir in 2010) (Barth et al. 2015). Across Yosemite, this compositional shift has especially affected large-diameter trees on long-unburned sites (Lutz et al. 2009a). Pre-fire surface fuel loads totaled 192.55 Mg ha^{-1}, distributed as < 1% 1-h fuels, 1% 10-h fuels, 2% 100-h fuels, 38% 1000-h and larger fuels, 13% litter, and 46% duff (Cansler et al. 2019).

The YFDP was burned during the Rim Fire as part of backfiring operations started on August 31, 2013. The backfire was lit approximately 1 km south of the plot. The fire backed downslope into the plot around 1:30 a.m. on September 1. The plot burned through the night and completed active burning by 11:30 on the morning of September 2. Fire effects were mixed, with a full range of fire severities represented (Blomdahl et al. 2019), but predominantly low and moderate severity effects (for more detailed burning characteristics, see Lutz et al. 2017). The fire consumed 79% of the total pre-fire surface fuel load (Cansler et al. 2019).

Spatial pattern predictor variables

We used pre-fire lidar-based measurements of structure and pattern to predict fire mortality. We used only lidar-based predictors so that the resultant model could be used to make predictions without additional ground measurements. We used lidar data acquired on July 21–22, 2010 by Watershed Sciences, Inc. of Corvallis, Oregon. Data were collected using dual-mounted Leica ALS50 Phase II instruments flown at 1300 m above ground level. Each instrument could capture up to 4 returns per pulse at a pulse rate ≥ 85 kHz with a ± 14° scan angle. Pulse density averaged 11 points m^{-2} across the acquisition (Fig. 1) with an increased density of > 30 points m^{-2} on the YFDP. Absolute survey accuracy was 4.4 cm root mean squared error. The vendor created and delivered a ground model using TerraScan and TerraModeler software (TerraSolid Oy, Helsinki, Finland).

We used individual tree detection methods described by Jeronimo et al. (2018) to process the lidar data into tree-approximate objects (TAOs). TAOs represent objects resolvable by lidar, each of which is a canopy tree along with any subordinate trees that may be hidden by the dominant tree's foliage (Jeronimo et al. 2018). All subsequent lidar analysis was done with R version 3.3.2 (R Core Team 2016).

We analyzed structure and mortality at three scales: the TAO, the local area, and the neighborhood. The local area refers to a virtual 0.1 ha circular plot (17.8 m radius) centered at the middle of each TAO. The neighborhood scale refers to 24 90 × 90 m subplots tiling the YFDP, with 10 m of buffer between subplots (Fig. 2a). We created predictor variables at each scale from the lidar point cloud, canopy height model, and TAO data.

To create predictor variables at the TAO scale we clipped the lidar point cloud by each TAO crown polygon and calculated the following point cloud statistics corresponding to structure: canopy cover in strata from 0–2 m, 2–4 m, 4–8 m, 8–16 m, 16–32 m, and > 32 m (Kane et al. 2013) and the height of the highest return. We calculated additional predictors based on published models for crown base height, crown fuel weight, crown bulk density, and leaf area index (Table 1). We recognize that these metrics may not correspond well to field measurements (Jakubowski et al. 2013; Kramer et al. 2014, 2016), but our exploratory analysis showed them to be useful and interpretable as relative indices. We estimated crown volume by idealizing each TAO crown as a paraboloid with crown length equal to TAO height minus estimated crown base height, and crown spread equal to the radius of a circle with an area equivalent to the TAO's footprint area (Fig. 2b). Lastly, we assigned each TAO membership in a clump following methods developed for stem maps by Larson and Churchill (2012) and adapted for TAOs by Wiggins et al. (2019) and Jeronimo et al. (2019), where TAOs are

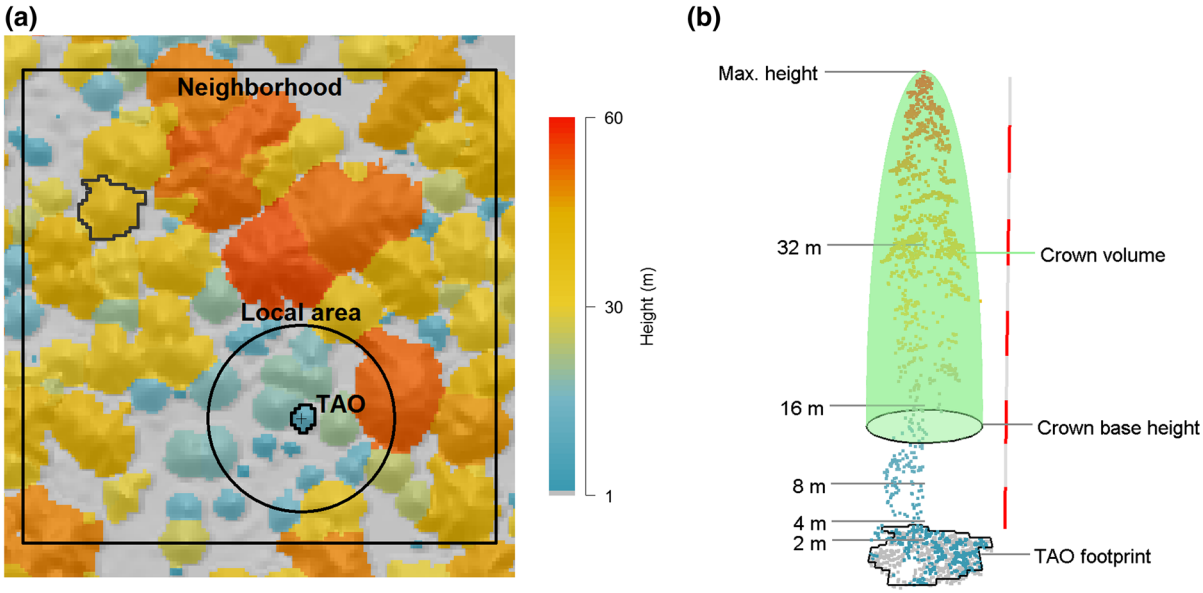

Fig. 2 **a** Schematic of scales used in this study. The TAO scale represents individual trees or closely grouped clusters of trees identified by lidar. The local area scale is a 0.1 ha circular plot placed around each TAO. The neighborhood scale is a 90 × 90 m fixed window. The Yosemite Forest Dynamics Plot was subdivided into 24 neighborhoods and 48 more neighborhoods were sampled centered on our validation plot dataset. **b** Annotated TAO point cloud clipped from dark grey outline in panel **a**. Canopy cover is calculated in bins shown by the markings on the left side. Crown volume is estimated using a paraboloid extending from the TAO high point to the estimated crown base (Table 2), and with a radius such that the circle shown at the crown base has an area equal to the TAO footprint. Height pole is in 5 m increments

Table 1 Models used to create some of the tree-approximate object-scale predictor variables

Structural metric	Crown base height (m)
Model form	$((3.254 + 0.13 \times P25 - 0.021 \times P90 - 0.039 \times CC) + 0.214)^2$
Ecoregion	East Cascades, Washington
Citation	Erdody and Moskal (2010)
Structural metric	**Crown fuel weight (kg ha^{-1})**
Model form	$\exp((-0.536 + 0.031 \times CC) \times 1.028) \times 1000$
Ecoregion	East Cascades, Washington
Citation	Erdody and Moskal (2010)
Structural metric	**Crown bulk density (kg m^{-3})**
Model form	$\exp((-3.696 + 0.025 \times P25 - 0.03 \times P50 + 0.029 \times CC) \times 1.032)$
Ecoregion	East Cascades, Washington
Citation	Erdody and Moskal (2010)
Structural metric	**Leaf area index (m^2 m^{-2})**
Model form	$-2.907 \times \ln(1 - CC)$
Ecoregion	Puget Lowlands, Washington
Citation	Richardson et al. (2009)

P25, *P50*, *P90* 25th, 50th, and 90th percentile lidar return heights, respectively, *CC* canopy cover, or proportion of lidar first returns with heights ≥ 2 m

considered members of the same clump if their high points are within 6 m of one another. We used clump size as an additional TAO-level predictor.

At the local area scale we calculated measures of density and canopy openings. We calculated TAO density within the 0.1 ha plot and estimated basal area using height–diameter regressions from Jeronimo et al. (2019). We quantified open space using the open space transform (Churchill et al. 2013, 2017); we overlaid a 0.5 m grid on each plot and calculated the distance from each grid cell center to the nearest TAO high point. We took the mean of these values for each 0.1 ha plot as an open space index.

Lastly, we calculated metrics for each 90 × 90 m neighborhood. We calculated TAO density, canopy cover < 2 m, and canopy cover ≥ 2 m. We used rumple (canopy surface roughness; Kane et al. 2010) as an index of structural complexity. To characterize spatial pattern we calculated the mean clump size and the proportion of neighborhood area > 9 m from a TAO high point, an index of open space (Jeronimo et al. 2019).

To correct for edge effects (i.e., TAOs spanning a neighborhood boundary and containing unsampled trees outside the neighborhood) we constrained modeling to use only TAOs whose high points were at least 5 m from the edge of the 90 × 90 m neighborhood. This removed 489 TAOs from analysis.

Topography, water balance, and burn weather predictors

We included topographic, water balance, and burn weather predictors for each neighborhood in the YFDP (and in the independent validation plots, below) since these variables have been shown to be important predictors of fire severity (Miller and Urban 1999; Kane et al. 2015b; Blomdahl et al. 2019). We used actual evapotranspiration and climatic water deficit data from Flint et al. (2014). We calculated slope at 30 m and 270 m scales and topographic position index at 500 m, 1 km, and 2 km scales (Weiss 2001; Kane et al. 2015b). We used FireFamilyPlus version 4.2 (USDA 2016) to calculate daily burning index, energy release component (ERC), maximum temperature, minimum relative humidity, and mean wind speed from the Crane Flat Weather Station, which is located < 1 km from the YFDP (Station ID 044,102) (Fig. 1). We assigned these values to each neighborhood according to the date of burning, which was taken from daily fire progression maps (Lydersen et al. 2014).

Fire mortality response variables

The YFDP was surveyed for tree mortality in each post-fire year 2014–2017, allowing determination of immediate mortality (dead by the time of May 2014 census) versus delayed mortality (alive in 2014 but dead by May 2017 census) and survivorship (alive at May 2017 census). Each tree was assigned one or more causes of mortality based on observable conditions. We only examined trees ≥ 10 cm dbh to match diameter cutoffs from commonly used fire mortality models (e.g., FOFEM; Ryan and Reinhardt 1988). This excluded 22,528 trees with $1 \leq$ dbh < 10 cm from our analysis. We removed 49 trees with mortality causes that were not directly attributable to fire (e.g., small trees crushed by falling debris). We did not consider trees that were dead pre-fire nor trees that showed very low vigor (imminent mortality) in the 2017 survey (n = 4358). An additional 2925 trees were situated within the buffer zones between neighborhoods and 1323 trees were removed from analysis due to the edge corrections.

In preliminary analyses we found that models predicting numbers of trees killed had more predictive power than models predicting proportions of mortality at TAO and neighborhood scales. Thus, we formulated model responses in terms of numbers of trees killed. To allow for indirect calculations of proportional mortality rates we also simultaneously modeled numbers of live trees pre-fire. The ratio of modeled mortality to modeled density can provide a normalized estimate of mortality rates.

We prepared response variables at two scales. At the TAO scale we counted the number of trees that were members of each TAO, matching mapped trees to TAOs by finding minimum distances between mapped trees and TAO high points (Jeronimo et al. 2018). We then partitioned these into counts of immediate mortality, delayed mortality, and survivorship for each TAO. At the neighborhood scale we calculated tree density (trees ha^{-1}) and mortality (trees ha^{-1}), without separating immediate from delayed mortalities.

Independent validation plots

We installed 48, 1/4-ha validation plots covering the full elevational and fire severity ranges of the Rim Fire in Yosemite where it was covered by the 2010 lidar acquisition (Fig. 1). The range of sampling for the validation plots included sites warmer and drier than the YFDP (generally more *Pinus ponderosa*-dominated) as well as cooler, wetter sites (generally more *Abies magnifica*-dominated).

Plots were located by random selection in clustered locations at least 100 m from a road or trail, but within 2 km of road or trail access. Plots were stratified a priori by satellite-derived burn severity as calculated by Blomdahl et al. (2019) (Fig. 1), and were installed in May to July 2017. Plots were 50 × 50 m squares oriented to the cardinal directions. One corner of each plot was geo-located using a Topcon HiPer V GPS recording at 1 Hz for an average of 60 min (range 17 to 120 min). The rooting location of each tree ≥ 10 cm dbh was measured and mapped whether it was alive or dead and either standing or down. Tree status was determined from visual cues such as remnant foliage, bole and basal charring and consumption, presence of pitch on the bole, and local soil burn severity, and was classified as either healthy, declining, nearly dead, recent non-fire mortality, immediate fire mortality, delayed fire mortality, or dead pre-fire. Field crew members drew from several years of experience evaluating tree mortality on the YFDP both pre- and post-fire to evaluate tree status.

For each validation plot we calculated lidar metrics on 90 × 90 m squares centered on the 50 × 50 m plot. Similar to the edge correction used for the YFDP data, we only included TAOs with high points at least 5 m from the edge of the plots. Together, the 24 90 × 90 m neighborhoods from the YFDP and the 48 neighborhoods from the validation plots spanned a wide range of conditions in terms of topography, water balance, and burn weather (Tables A1, A2).

Statistical analysis

We modeled post-fire tree mortality as a set of four generalized linear models in a Bayesian framework (Table 2). At the TAO scale, we modeled the number of trees per TAO partitioned into immediate mortality, delayed mortality, and survivors. At the neighborhood scale we modeled the total number of mortalities, first using only structural predictors and then additionally including topography, water balance, and burn weather predictors. Lastly, we tested a formulation of the full model that was hierarchically structured across scales compared to separate models for each scale. The hierarchically structured model included an interaction term between number of trees killed at the neighborhood level and the TAO level (Fig. 3; see Online Resource 1 for complete model definitions).

Table 2 Four tree mortality model formulations tested

Model	Structural predictors	Topography, water balance, and burn weather predictors	Cross-scale linkage
S	Yes	No	No
ST	Yes	Yes	No
SL	Yes	No	Yes
STL	Yes	Yes	Yes

See text Statistical analysis section for a description of the different components. See Fig. 2 for a graphical representation of modeling relationships

We combined the validation plots with the YFDP data for the neighborhood-level modeling to capture more representative ranges of variation because variation in topography, water balance, and burn weather was low across the YFDP relative to variation that occurs across the Sierra Nevada mixed-conifer zone. For the TAO-scale models, however, we used only the YFDP data and retained the validation plots as an independent testing data set.

Neighborhood-level models used 72 neighborhoods, 2620 TAOs and associated local areas, and 10,767 trees ≥ 10 cm dbh. Sample sizes for the TAO-level models, which did not include the validation plots, were 24 neighborhoods, 1773 TAOs and local areas, and 7488 trees ≥ 10 cm dbh.

We estimated posterior distributions of parameters for all models using JAGS 4.2.0 Markov chain Monte Carlo sampling software (Plummer 2003, 2016a) within the rjags package (version 4.6; Plummer 2016b) in the R environment (version 3.3.2; R Core Team 2016). For initial testing each model was run with two chains, 500 adaptation iterations, 500 burn-in iterations, and 5000 sampling iterations. Convergence was judged based on visual assessment of the posterior distributions for the model coefficients and by the Gelman–Rubin diagnostic (accepted at values ≤ 1.1; Gelman and Rubin 1992). Parameters were estimated

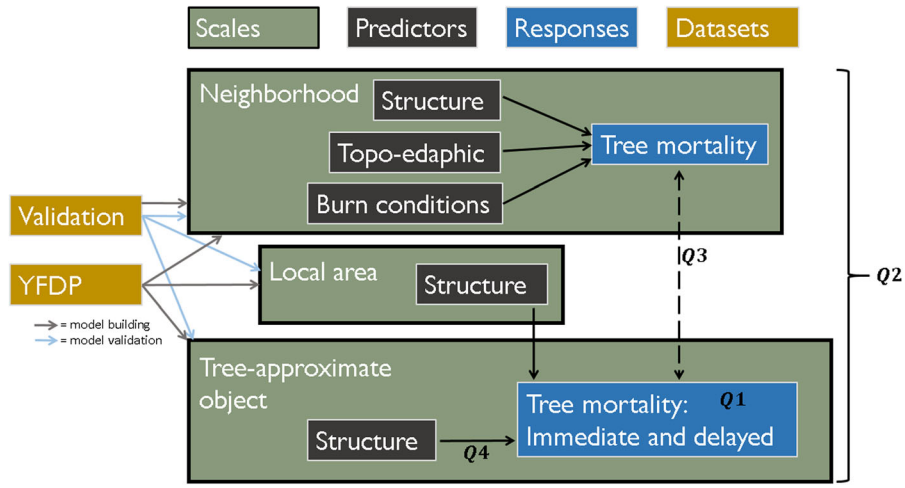

Fig. 3 Flowchart of data sources, conceptual formulation of mortality model, and relationships to study questions. For the data sources, the Yosemite Forest Dynamics Plot (YFDP) dataset was used to create models at all three scales, while the validation plot dataset was used to build the neighborhood level models and to validate models at all scales. In the model schematic, black arrows represent explanatory variables being used to predict a response variable, while the dashed arrow between response variables represents a cross-scale linkage where an interaction term was included between neighborhood-level mortality and TAO-level mortality. Models were tested both with and without this term. Labels Q1–Q4 represent the four study questions: labels are placed next to the data source, interaction, or model analyzed to answer each question

as the mean of the combined distributions of the two chains. We used posterior predictive checks to confirm that the posterior distributions represented the data well (Gelman et al. 2004); Bayesian *p*-values were all between 0.45 and 0.55.

We used a stochastic search variable selection (SSVS) procedure (George and McCulloch 1993) to narrow down the list of variables used in the models (Online Resource 1). This procedure pairs each predictor with a Bernoulli-distributed inclusion parameter that indicates whether the variable is a likely predictor for each link in the Monte Carlo chain given the observed data. The posterior estimates for the Bernoulli distributions' inclusion parameters represent the proportion of links where the given variable was a likely predictor, and can be interpreted as importance values. We tuned the SSVS to select four predictors per link on average.

We selected the final set of models from among the tested options (Table 2) using two criteria. For the TAO-level models, which had separate training and testing data, we used the log predictive density scoring function (LPD; Gelman et al. 2014) to select the best model. For the neighborhood-level models, which did not have separate training and testing data, we used the posterior predictive loss function (D_{sel}; Gelfand and Ghosh 1998). After choosing a model form with these criteria, we chose subsets of predictor variables by iteratively removing those with the lowest importance values until all predictors were included in at least 60% of Monte Carlo links.

We performed final model runs using the same procedures described above for the model selection runs, but with three chains, 2000 adaptation iterations, 2000 burn-in iterations, and 20,000 sampling iterations. We then evaluated absolute accuracy by calculating the root mean squared prediction errors on both training and testing datasets.

Mechanistic interpretation of model results

We took the most important predictor at each of the TAO and local area scales to investigate possible mechanisms through which these structural characteristics affect fire mortality at fine scales. We stratified the range of each of these predictor variables into 10 bins so that each bin contained an approximately equal number of trees. We compiled the list of factors associated with mortality—of which each tree could have several—for each bin and normalized this list to

sum to one to get proportions of mortality factors in different categories.

For immediate mortalities we used the following categories of mortality agents: suppression, pathogen (almost all root rots of genus *Armillaria*), beetle (genera of *Scolytinae*), mechanical, fire crown damage, fire stem damage, and fire-induced mechanical collapse, the latter of which refers to trees that suffered mechanical failures due to combustion of structural tissue (generally heartwood). Fire crown damage and fire stem damage almost always were recorded together; to help differentiate between them we only included the one that was recorded as more severe in the field survey. For delayed mortalities we first compared fire-related factors to non-fire related factors, then evaluated relative proportions of non-fire-related factors alone.

We took these mortality proportion data to represent contingency tables (i.e., a matrix where each cell gives the number of mortalities related to a given agent within a given structural stratum). We calculated χ^2 statistics for these tables and performed an iterative procedure to reduce the 10 bins to the two most highly contrasting bins possible. At each step we tested every pair of adjacent bins to see which yielded the highest χ^2 statistic when combined. We repeated this until we were left with only two bins, ensuring that the χ^2 statistic was significant at each step. From this we were able to identify a threshold for each of the structural predictors tested along with an effect on causes of mortality at that threshold.

Results

Immediate and delayed mortality in the YFDP

Of trees $\geq$ 10 cm DBH in the YFDP that were alive in 2013 (n = 11,974), 39% died immediately after fire, 24% died 2–4 years post-fire, and the remaining 37% were alive in May 2017. Mortality decreased over time: 62% of mortalities occurred in the first year (2013–2014) followed by 22% in the second year, 12% in the third year, and 4% in the fourth year. Mortality rates decreased similarly, with a rate of 39% the first year, 23% of remaining live trees the second year, 16% the third year, and 6% the fourth year (Fig. 4). In general, smaller trees died either in the fire or soon thereafter and larger trees died in later years

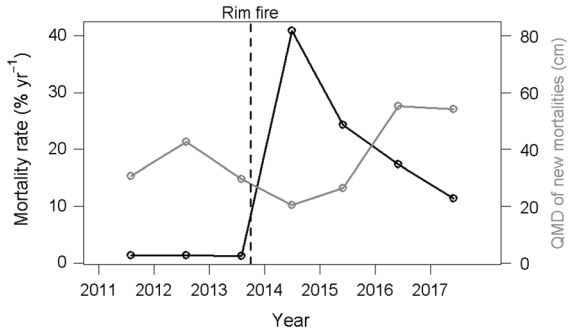

Fig. 4 Rates and demographics of tree mortality for trees $\geq$ 10 cm dbh on the Yosemite Forest Dynamics Plot (YFDP) for three pre-fire censuses and four post-fire censuses. *QMD* quadratic mean diameter. Point locations on the *x*-axis are resolved to the month of each annual census. The vertical line representing the Rim Fire is on August 31, 2013, the date when the Rim Fire entered the YFDP

(Fig. 4). The quadratic mean diameter of trees that died in the first year was 21.0 cm, followed by 27.6 cm in the second year, 57.8 cm in the third year, and 55.1 cm in the fourth year. Proportional mortality rate estimates and pre-fire density models are reported in Online Resource 1.

Validation plots

The 48 validation plots spanned from 1430 to 2250 m elevation and covered forest types ranging from low montane *P. ponderosa–Quercus chrysolepis* to high montane *A. magnifica* (Table A3). Density of trees $\geq$ 10 cm dbh ranged from 85 to 1005 trees ha^{-1} and basal area ranged from 14 to 122 m^2 ha^{-1}. Species included all those found in the YFDP as well as *Pinus contorta*, *P. jeffreyi*, and *Q. chrysolepis*. Mortality was estimated as 56% immediate and 44% delayed after applying a correction factor (Online Resource 2). In total, 5686 trees were sampled on the validation plots of which 3279 were included for analysis after the edge correction.

Model results

At the neighborhood scale, including the selected water balance and burn predictors had the largest effect on accuracy, improving D_{sel} values by 54% (Model S vs. Model ST) (Table 3). In contrast, including the cross-scale linkage (Models SL, STL)

Table 3 Model assessment statistics for the four tested model formulations

Neighborhood scale	Model	D_{sel}	RMSE (trees ha^{-1})		
			Immediate mortality	Delayed mortality	Total mortality
	S	926,699	78.7	63.4	89.4
	ST	426,853	70.8	44.3	84.8
	SL	924,992	76.8	63.4	89.4
	STL	***426,432***	***70.1***	***43.9***	***84.4***

Tree-approximate object scale	Model	LPD	RMSE (n trees)			
			In-sample		Out-of-sample	
			Immediate mortality	Delayed mortality	Immediate mortality	Delayed mortality
	S	− 5716	1.693	1.759	1.898	1.388
	ST	− 5394	1.693	1.759	1.897	***1.387***
	SL	− 4842	1.638	1.734	1.886	1.398
	STL	***− 4793***	***1.613***	***1.706***	***1.885***	1.403

The best statistic for each column is in bold italic face

RMSE root mean squared error, D_{sel} posterior predictive loss function (Gelfand and Ghosh 1998), where lower numbers represent a better and more parsimonious model fit, *LPD* log predictive density (Gelman et al. 2014), where higher (less negative) numbers represent a better and more parsimonious model fit

Table 4 Predictors selected for the final models, importance values from the stochastic search variable selection (George and McCulloch 1993), and signs of predictor relationships to mortality and survival

Sub-model	Predictor	Importance value	Sign		
Neighborhood mortality	Actual evapotranspiration (mm H_2O year^{-1})	1.00		+	
	Open space (proportion)	1.00		−	
	Energy release component (BTU ft.$^{-2}$)	0.99		−	
	Maximum burn day temperature (°C)	0.96		+	
	Canopy cover > 2 m (%)	0.88		+	
	Rumple (m^2 m^{-2})	0.80		+	
			I	D	S
TAO immediate mortality	Maximum height (m)	1.00	−	+	+
	Canopy cover < 8 m (%)	1.00	+	−	−
	Mean clump size in local area (*n* TAOs)	0.99	+	−	−
	Local area open space (%)	0.89	−	−	+
	Leaf area index (m^2 m^{-2})	0.73	+	+	−
TAO delayed mortality	Local density (TAOs ha^{-1})	1.00	+	+	−
	Canopy cover 8–16 m (%)	0.99	−	+	+
	Canopy cover < 2 m (%)	0.99	+	−	−
	Crown fuel weight (kg)	0.88	−	−	+
	Crown base height (m)	0.86	−	+	+

Importance values represent the proportion of times in a Monte Carlo chain that the variable in question was selected to be included in the model, based on the likelihood of the predictor variable given the observed data. For the TAO-level models, which had trinomial responses, signs are reported for each response category (*I* immediate, *D* delayed, *S* survival). Note that energy release component is expressed in non-standard units. One BTU ft.$^{-2}$ is equal to approximately 11.357 kJ m^{-2}

had only a minute effect on the neighborhood-level models (< 0.2%). Model STL, which included topography, water balance, and burn weather predictors as well as the cross-scale linkage, performed best overall (Table 3). The top predictors for this model were AET, open space, ERC, maximum burning day temperature, canopy cover > 2 m, and rumple (Table 4). Root mean squared prediction error (RMSE) was 70 trees $ha^{-1} \geq 10$ cm dbh.

In contrast to the neighborhood-level models, the cross-scale linkage had a substantial effect on TAO-level mortality models, improving the LPD value by 18% (Model S vs. Model SL). Including topography, water balance, and burn weather predictors had a smaller effect, improving LPD by 6% (Model S vs. Model ST) (Table 3). Like the neighborhood models, Model STL performed best at the TAO scale. The top predictors for the immediate mortality component of this model were maximum TAO height, canopy cover < 8 m, mean clump size in local area, open space in local area, and leaf area index. The number of delayed mortalities was best predicted by local TAO density, canopy cover 8–16 m and < 2 m, crown fuel weight, and crown base height (Table 4). When predicted back on the YFDP training data, the number of immediate mortalities ≥ 10 cm dbh per TAO had an RMSE of 1.6 trees and the number of delayed mortalities had an RMSE of 1.7 trees. Predicting on the out-of-sample validation plots, RMSE for number of immediate mortalities ≥ 10 cm dbh was 1.9 trees and RMSE for delayed mortalities was 1.4 trees. When these numbers were summarized up to the neighborhood scale, the RMSE for immediate mortalities ≥ 10 cm dbh was 70.1 trees ha^{-1} and was 43.9 trees ha^{-1} for delayed mortalities (Table 3). See Online Resource 1 for fitted model coefficients.

Relationships between fine-scale structure and mortality agents

Immediate mortalities were overwhelmingly fire-related, with nearly 98% of mortality factor records attributed to fire crown damage, fire stem damage, and fire-mechanical damage (n = 1321). At the TAO scale, the proportion of mortalities attributed to crown damage was higher when the dominant canopy of a TAO was < 51 m tall (74% vs. 66%; $p < 0.001$). The increase in crown damage mirrored a decrease in stem damage of similar magnitude (Fig. 5). At the local area scale, crown damage decreased and stem damage increased by five percentage points when mean clump size was > 23 TAOs ($p < 0.05$). Fire-mechanical mortalities (total n = 12) were five times more common when TAO height was > 51 m (4 vs. 20 tree mortality events) and when local area mean clump size was > 23 TAOs (6 vs. 31 tree mortality events) (Fig. 5).

Delayed mortalities also were dominated by fire-related mortality factors (71%, n = 1206). At the TAO scale the proportion of mortality factor records that were fire-related was 14 percentage points lower when crown base height was > 28 m ($p < 0.001$). At the local area scale fire-related mortality was 22 percentage points higher when TAO density was > 170 ha^{-1} ($p < 0.001$) (Fig. 5).

Of the non-fire related factors, bark beetles and pathogens accounted for the most mortality, 46% and 34% respectively, followed by suppression with 16% of mortality records and mechanical damage with the remaining 4%. When TAO crown bases were higher than 18 m, beetle mortalities were 11 percentage points higher, pathogen mortalities were 7 percentage points lower, and mechanical mortalities decreased from 6.4 to 2.7% ($p < 0.001$). Suppression mortalities did not differ with crown base height. At the local area scale, TAO densities greater than 180 ha^{-1} were associated with less beetle kill (48% reduced to 23%), more pathogenic mortality (32% to 50%), and more suppression (15% to 22%). The share of mortalities attributed to mechanical damage did not differ with TAO density.

Discussion

We found that patterns of post-fire tree mortality are driven by multiple factors interacting across scales. A theory of cross-scale interactions has been developed for fire regimes (Heyerdahl et al. 2001; Falk et al. 2011; Parks et al. 2012; Merschel et al. 2018), but has not been described for fire effects within an individual fire. As fire moves contagiously across a landscape its ultimate effects are determined by a complex of processes occurring at and interacting between multiple scales (Falk et al. 2007; McKenzie and Kennedy 2011). This study represents a step in the development of the landscape ecology of fire and suggests that formalizing the hierarchical structure of

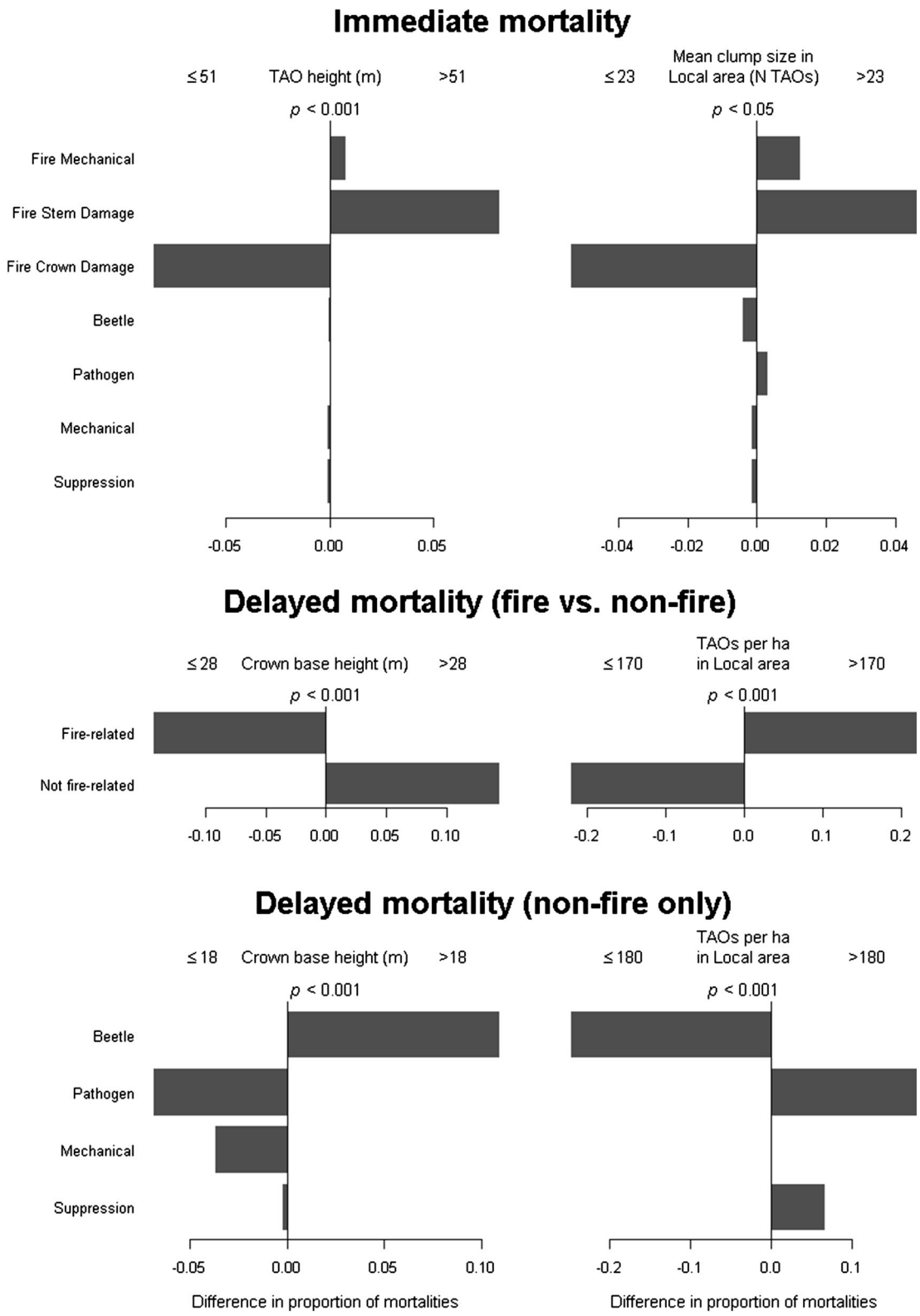
Immediate mortality
≤ 51
TAO height (m)
>51
p < 0.001
Fire Mechanical
Fire Stem Damage
Fire Crown Damage
Beetle
Pathogen
Mechanical
Suppression
-0.05
0.00
0.05
≤ 23
Mean clump size in
Local area (N TAOs)
>23
p < 0.05
-0.04
-0.02
0.00
0.02
0.04
Delayed mortality (fire vs. non-fire)
≤ 28
Crown base height (m)
>28
p < 0.001
Fire-related
Not fire-related
-0.10
-0.05
0.00
0.05
0.10
≤ 170
TAOs per ha
in Local area
>170
p < 0.001
-0.2
-0.1
0.0
0.1
0.2
Delayed mortality (non-fire only)
≤ 18
Crown base height (m)
>18
p < 0.001
Beetle
Pathogen
Mechanical
Suppression
-0.05
0.00
0.05
0.10
Difference in proportion of mortalities
≤ 180
TAOs per ha
in Local area
>180
p < 0.001
-0.2
-0.1
0.0
0.1
Difference in proportion of mortalities

◀**Fig. 5** Relationships between structural predictors of tree-approximate object (TAO)-scale mortality and agents of mortality in three categories: immediate mortality, delayed mortality comparing fire-related mortality agents to non-fire agents, and delayed mortality comparing among only non-fire agents. For each category the left-hand chart shows the most important predictor measured at the TAO scale and the right-hand chart shows the most important predictor measured at the local area scale (see Fig. 2). For each predictor we identified the threshold that best differentiated between mortality agents. The charts show the difference in proportions of mortalities attributed to each agent between trees in TAOs above the threshold versus TAOs below the threshold. For example, when a bar points to the left, it means the associated mortality agent is more prevalent for trees in TAOs below the given threshold

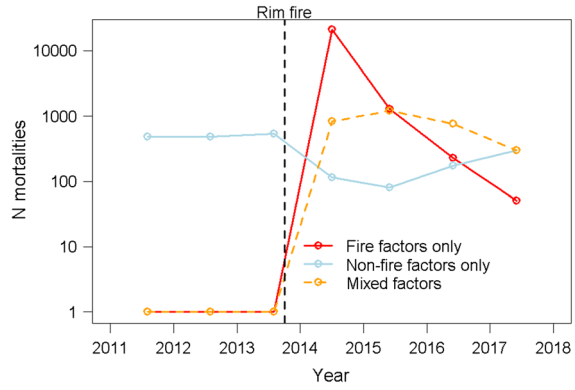

Fig. 6 Predominance of mortality factor classes for trees ≥ 10 cm dbh on the Yosemite Forest Dynamics Plot (YFDP) for three pre-fire censuses and four post-fire censuses reported on the basis of individual trees. "Fire factors only" refers to trees that had no observable conditions contributing to death except fire damage, "non-fire factors only" refers to trees that had no observable fire damage, and "mixed factors" refers to trees for which both fire-related and non-fire related conditions contributing to death were observed. Point locations on the *x*-axis are resolved to the month of each annual census. The vertical line representing the Rim Fire is on August 31, 2013, the date when the Rim Fire entered the YFDP

landscapes in empirical models is a productive way to advance the ecological understanding of disturbance processes.

Mortality rates and agents over time

Most mortality on the YFDP occurred in the first year (62% of mortalities compared to 55–90% in the literature) and subsequent years showed monotonically decreasing amounts of tree death (Fig. 4) (Keyser et al. 2006; Hood and Bentz 2007; Hood et al. 2010; Prichard and Kennedy 2012). First-year mortality occurred disproportionately in small trees and mortality in subsequent years advanced through larger diameter classes (Fig. 4) (Breece et al. 2008; Youngblood et al. 2009; Van Mantgem et al. 2011).

Previous work has suggested that immediate mortality is due mainly to direct fire effects—i.e., crown and cambium damage—while delayed mortality is due to stress from non-lethal damage predisposing trees to other agents of mortality (Youngblood et al. 2009; Woolley et al. 2012; Smith et al. 2016). This explains the advance of mortality from small trees to larger trees over time, since larger trees more likely to be damaged than immediately killed by direct effects and because agents of delayed mortality, particularly bark beetles, tend to favor larger trees (Breece et al. 2008; Hood et al. 2010; Jenkins et al. 2014). Our results partially support this model, but suggest additional complexity. For example, we observed many instances of fire damage to vascular and foliar tissue leading to mortality 2–4 years post-fire with no other apparent mortality agents (Fig. 6). This delayed first-order mortality is likely due to the death of fine roots limiting the amount of water available to the crown, which can either be caused by direct damage to fine roots (O'Brien et al. 2010) or by phloem death low on the bole prohibiting photosynthate from reaching the roots (Hood 2010).

Model accuracy

The accuracy of modeling post-fire tree mortality based on pre-fire structure measurements is limited due to the stochasticity of fire as a physical process (Furniss et al. 2019). For example, at scales of tens of thousands of hectares, Kane et al. (2015b) predicted fire severity at a 30 m grain size resulting in a pseudo-r^2 value of 0.50 and Lydersen et al. (2017) created a similar model with a pseudo-r^2 value of 0.46. At finer scales, Furniss et al. (2019) predicted death of individual trees from pre-fire structure with accuracies ranging from 75 to 88%. In comparison, our neighborhood-level mortality model had an r^2 value of 0.67 and our TAO-level immediate mortality and delayed mortality models had r^2 values of 0.55 and 0.48, respectively. We suspect the disparity in accuracy between scales may be driven by errors in assigning field-measured trees to lidar-identified TAOs. TAOs are, by nature, roughly defined and it can be difficult

definitively match a stem map with a TAO map. However, there is much more certainty when delineating which trees occur within a neighborhood, since the neighborhoods we used contain greater interior space than a TAO does. Thus, the accuracy of the response variables (numbers of trees killed) may be a major differentiating factor in model accuracy between scales.

Model accuracy certainly would improve with the inclusion of species composition data; however, accurate mapping of species composition is presently not possible at the same scale and resolution as is possible for lidar structure data. Other potential predictors that may have improved model accuracy include shrub cover (Lutz et al. 2017), multi- or hyperspectral orthoimagery and derived indices, and higher spatial and temporal resolutions of burning weather data. None of these data were available for our study area and, indeed, are not commonly available with or derivable from lidar.

An important characteristic of the selected model (Model STL) is that accuracy in terms of RMSE was nearly identical for predictions on in-sample training data compared to predictions on out-of-sample testing data (Table 3). Our validation plot dataset, which was not used to fit TAO-level models, covers a wide range of environmental conditions spanning the diversity of elevation, aspect, and fire severity that the Rim Fire burned through in Yosemite. The fact that predictions on this dataset are similarly accurate to predictions on the geographically constrained training dataset indicates that the model properly captures some mechanisms driving tree mortality and can be applied throughout the mid-montane Sierra Nevada mixed-conifer zone, within the environmental bounds captured by our validation plots.

Multi-scale drivers of fire mortality

The neighborhood-scale mortality predictors fell into three categories: fuel amounts, fuel configuration, and burn weather (Table 4; Fig. 7). Canopy cover and AET are correlated with fuel amounts, where canopy cover gives the amount of canopy fuels and AET is related to site productivity and thus shrub and herb fuel loads as well as proportions of shade-tolerant understory trees (Lutz et al. 2010; Kane et al. 2015b). Fuel configuration was characterized by open space proportion and rumple, which are measures of overstory fuel breaks and canopy complexity, respectively (Kane et al. 2010, 2014). Burn weather was characterized by maximum temperature on burn day and ERC. Surprisingly, higher ERC values were associated with less mortality (Table 4), contradicting previous findings using this index (Williams et al. 2015; Lydersen et al. 2017). The most likely explanation for this is that all neighborhoods burned at relatively high ERC values—92% over the high-severity threshold of 72 identified by Lydersen et al. (2017) (Table A2)—and so ERC acted as an interactive term damping the effect of the highest maximum temperatures. Topographic predictors like slope and topographic position were not themselves important predictors, but do affect AET. This suggests that the importance of topography was mainly expressed through its role in modulating growing conditions, and that the influence of burn weather on fire severity was greater than the influence of topography.

Mortality predictors at the TAO scale fell into categories of fuel connectivity, fire tolerance, and local stress (Fig. 7). Conditions in these categories acted as a series of filters determining whether a tree escaped fire damage, died immediately, died 2–4 years post-fire, or recovered. Fuel connectivity was represented in the immediate mortality model by canopy cover < 8 m, local area open space, and mean clump size in local area and in the delayed mortality model by canopy cover < 2 m, canopy cover 8–16 m, and crown base height. These factors indicate different aspects of surface and understory fuels, ladder fuels, and horizontal canopy fuel breaks. Trees situated within TAOs and local areas with low vertical and horizontal connectivity were more likely to survive, probably because they experienced less initial fire damage. Fire tolerance determined whether a tree died immediately or went on to experience delayed mortality. This was indicated by TAO height, since larger trees are more likely to survive fire by virtue of their thicker bark and greater access to resources (Ryan and Reinhardt 1988; Hood et al. 2007; Furniss et al. 2019), and TAO leaf area index, where a high value usually indicates the presence of shade-tolerant, fire-intolerant species (Lusk 2002; Gersonde and O'Hara 2005). Lastly, local stress conditions predicted the amount of delayed mortality. These predictors were density in the local area and crown fuel weight. Local TAO density represents nearby competition for moisture resources, a major mortality factor in the Sierra Nevada (Young

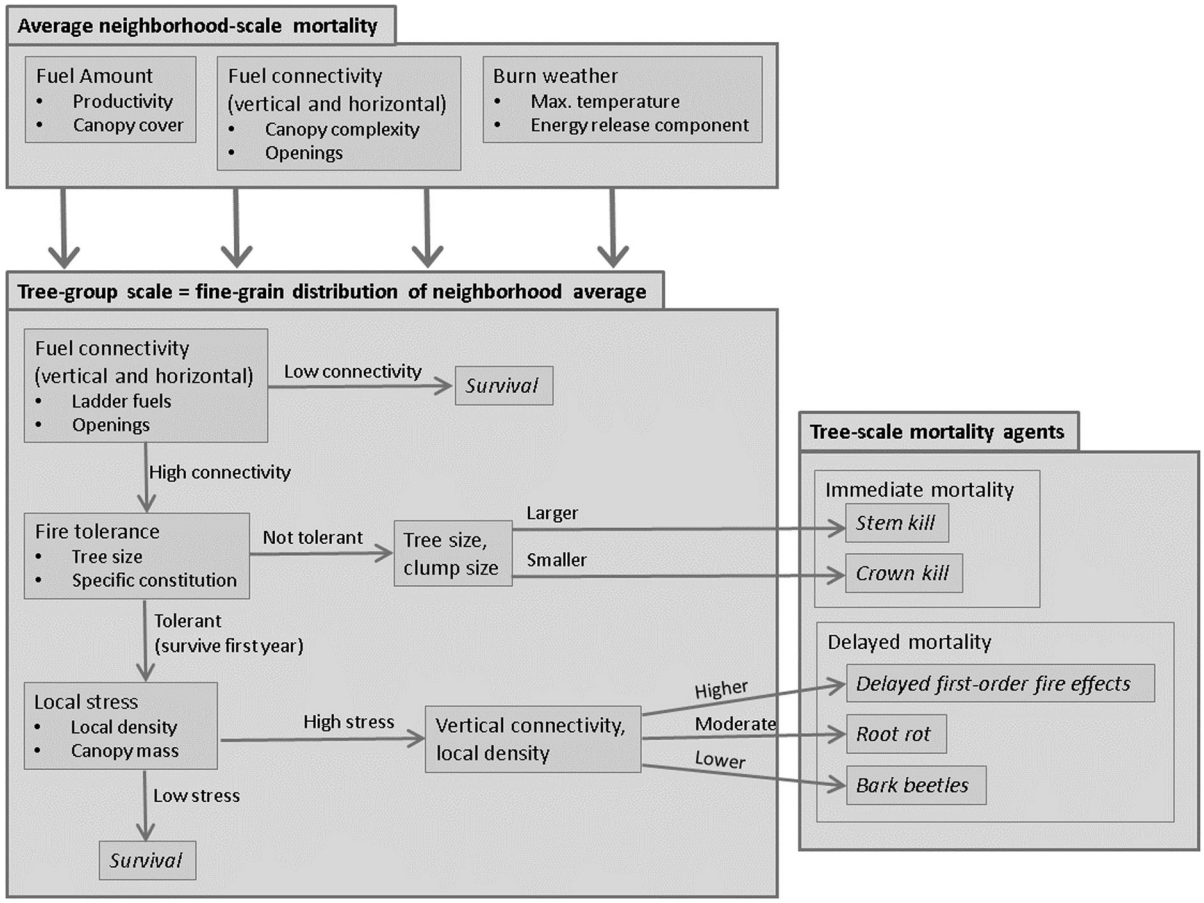

Fig. 7 Conceptual representation of study results. Post-fire tree mortality is driven from broader scales to finer scales, where fuel and burn weather attributes at the 90 × 90 m neighborhood scale determine the total amount of mortality and factors at the scale of small groups of trees determine the spatial distribution of that mortality. The process of post-fire mortality at the tree-group scale can be conceptualized as a series of filters. Fine-scale fuel connectivity determines a given tree group's risk of fire mortality. For tree groups with high fuel connectivity, fire tolerance determines first-year survival and local stresses determine longer-term survival. The actual mechanisms of death vary based on timing and fine-scale structure

et al. 2017). We expected that higher crown fuel weights would be associated with more mortality, but we observed the opposite relationship (Table 4). This emphasizes the "series of filters" concept: if a tree has low local fuel connectivity, then high crown fuel weight may simply indicate the large, healthy crown of a tree that is prepared to persist through stresses.

We recognize that our use of lidar as the primary predictive data source limits our ability to fully characterize fuel matrices. We included various measures of cover in and below the main canopy as predictor variables to represent amounts of material in lower fuel strata above the ground surface. These metrics can characterize certain surface fuels such as tall grasses, seedlings/saplings, shrubs, large woody debris ($\geq$ 1000-h), and $<$ 1000-h woody fuels that are supported above the ground, but cannot capture others such as litter, duff, twigs, and branches that sit directly on the ground surface. Due to the complex fire history of our study area, correspondence between surface fuel loads and proxies such as time since fire or overstory structure are likely to be weak and idiosyncratic. Although this study does not attempt to explicitly quantify the contributions of certain surface fuels, the models reported here nevertheless do have explanatory power for describing the post-fire tree mortality process.

Including cross-scale linkages between neighborhood-level and TAO-level models substantially improved model fits (Table 3). This aligns with the theoretical understanding of fire's landscape ecology, where different scales rest within a hierarchical structure with cross-scale interactions (Kotliar and Wiens 1990; Hessburg et al. 2015). The degree of improvement realized at the TAO scale was more than at the neighborhood scale, suggesting that cross-scale interactive drivers of fire severity exert a stronger influence from broader to finer scales than the reverse. This agrees with past studies that have identified weather and climatic water balance as the most important drivers of fire severity, upon which variation due to finer-scale structure is arranged (Gill and Taylor 2009; Lutz et al. 2009b; Kane et al. 2015b; Lydersen et al. 2017). However, spatial configuration of fuels at the neighborhood scale was also an important driver: Model SL performed nearly as well as Model STL for TAO mortality, despite not including topography, water balance, or burn weather predictors (Table 3). It appears that, rather than fine-scale effects integrating up to form a broad-scale result, the broad-scale conditions instead form the basic template that undergoes local modifications according to fine-scale conditions.

Relationships between fine-scale structure and mortality agents

For immediate mortalities, trees within taller TAOs and trees within larger clumps suffered less crown damage and more stem damage (Fig. 5). This could be because the shade under spreading tree crowns and within large clumps excludes understory vegetation; however, it could also be that larger trees and trees in clumps experienced similar levels of damage to smaller trees in smaller clumps but were able to recover better. Larger trees have more developed root systems and are more resilient to damage, and trees in clumps have mutually supportive root grafting and mycorrhizal relationships that can help provide clump-level resilience (Warren et al. 2008; Simard 2009; Salomón et al. 2016). It is also possible that trees within larger clumps are less exposed to convection currents that carry damaging heat into the canopy, i.e., local structural homogeneity encourages laminar subcanopy convection fields instead of turbulent vertical mixing (Smith et al. 2016; Parsons et al. 2018).

Of delayed mortalities occurring 2–4 years post-fire, 35% had no indications of mortality agents other than fire damage and 71% of mortality factors in total were fire-related. Higher crown base heights shifted the balance of delayed mortality causes away from fire effects. This was expected since fire effects should be more severe when there is more live biomass near the surface available to be injured or killed during fire and to potentially carry flames into the canopy. An interesting result is that the amount of fire-related mortality was higher in high-density local areas. This indicates that recovery from first-order fire damage, even without subsequent stresses by beetles, pathogens, or mechanical damage, is density-dependent and specifically is counteracted by high local density.

Associations between fine-scale structure and non-fire delayed mortality agents took the form of tradeoffs between mortality dominated by pathogens and mortality dominated by beetles. Deep crowns and high TAO density were associated with more mortality due to pathogens, whereas the balance shifted toward beetle kill when crown bases were high and local density was low to moderate (< 180 trees ha^{-1}). This dynamic may be due to structural correlates of species composition. Deep crowns and high density are typical of *A. concolor*, which is the species most often killed by pathogenic mortality, while high crown bases and lower stem density are attributes of larger *P. lambertiana* which are the primary host of tree-killing bark beetles in this study area.

Scaling up

Although the spatial extent of this study covered tens of thousands of hectares and included a wide range of environmental conditions, we did not explicitly analyze processes occurring at scales larger than the 90×90 m neighborhood. Our analysis captured the variation that may occur at the 1000–10,000 ha scale by virtue of plot placement. However, we did not capture processes like day-to-day fire spread, which can be driven by synoptic weather patterns and watershed-scale topography. Other research focusing on these scales suggests that the pattern we observed—significant effects acting from broader to finer scales—would hold upon expanding the hierarchy of scales to include larger scales like watersheds (Gill and Taylor 2009; Collins 2014; Lydersen et al. 2017).

Despite the relatively local scale of this study our findings have implications for landscape ecology in general, including studies of much larger landscapes. For one, we found that aligning model structure with landscape ecology theory produced a quantitatively better model and allowed for more insightful inference within the theoretical framework. The discipline of landscape ecology is premised on viewing ecosystems as hierarchical systems with cross-scale interactions; this study makes a compelling case for building models that reflect this premise.

Conclusions

Post-fire tree mortality is a complex process that depends on a variety of factors at many scales. We found that variation in mortality at the scale of trees and small groups of trees is arranged according to landscape-scale controls exerted by burn weather and fuel amounts and configurations at the 90 × 90 m neighborhood scale (Fig. 7). Within the neighborhood context, whether a given tree was killed immediately, died after a number of years, or survived the fire depended on a series of conditions: tree stature, initial fire effects, acute fire tolerance, and chronic stresses. All of these factors tend to be spatially heterogeneous and, in Sierra Nevada mixed-conifer forests, are patchily distributed (Lutz et al. 2013, 2018b). This emphasizes the importance of incorporating spatial patterns and spatial context when studying fire effects on vegetation. These ideas can also be incorporated into restoration treatments aimed at modifying fire behavior and effects (North et al. 2009; Churchill et al. 2013; Maher et al. 2019).

Our analysis of links between structural conditions and mortality agents revealed that structural conditions associated with resistance to one type of mortality agent often indicate susceptibility to another agent (Fig. 5). This suggests that landscape-scale heterogeneity in forest structure can provide a spatial balance of resistance to different mortality agents, and thus could be an important element of landscape stability and multi-scale resilience.

Acknowledgements We thank Brian Harvey, Monika Moskal, and Abby Swann for assistance with study design and manuscript preparation. We thank Alina Cansler and Sharon Hood for advice on interpretations of model results. We thank Bob McGaughey, Jonathan Kane, and Tristan O'Mara for assistance with lidar tool development and processing. We thank Tucker Furniss for assistance with creating Fig. 1 and for design and implementation of field protocols. We thank Etta Crowley, Dustin Mutch, Giulio DeFazio, Sara Germain, and Obi Germain for field work, as well as the hundreds of volunteers on the Yosemite Forest Dynamics Plot, credited individually at https://yfdp.org. Miles LeFevre and Russell Kramer provided comments on previous versions of this manuscript. This work was supported by the Joint Fire Science Program through Grant 16-1-04-02, "Using multi-scale spatial data to improve predictions of immediate and delayed post-fire mortality." Support for the Yosemite Forest Dynamics Plot is provided by the Utah Agricultural Experiment Station (Projects 1153 and 1398). This work was performed under National Park Service Research Permits YOSE-2013-SCI-0012, YOSE-2014-SCI-0005, YOSE-2015-SCI-0014, YOSE-2016-SCI-0006, YOSE-2017-SCI-0009, and YOSE-2018-SCI-0006 for studies YOSE-0051 and YOSE-2017-SCI-0008.

References

Agee JK, Skinner CN (2005) Basic principles of forest fuel reduction treatments. For Ecol Manag 211:83–96

Anderson-Teixeira KJ, Davies SJ, Bennett AC, Gonzalez-Akre EB, Muller-Landau HC, Wright SJ, Abu Salim K, Almeyda Zambrano AM, Alonso A, Baltzer JL, Basset Y, Bourg NA, Broadbent EN, Brockelman WY, Bunyavejchewin S, Burslem DFRP, Butt N, Cao M, Cardenas D, Chuyong GB, Clay K, Cordell S, Dattaraja HS, Deng X, Detto M, Du X, Duque A, Erikson DL, Ewango CEN, Fischer GA, Fletcher C, Foster RB, Giardina CP, Gilbert GS, Gunatilleke N, Gunatilleke S, Hao Z, Hargrove WW, Hart TB, Hau BCH, He F, Hoffman FM, Howe RW, Hubbell SP, Inman-Narahari FM, Jansen PA, Jiang M, Johnson DJ, Kanzaki M, Kassim AR, Kenfack D, Kibet S, Kinnaird MF, Korte L, Kral K, Kumar J, Larson AJ, Li Y, Li X, Liu S, Lum SKY, Lutz JA, Ma K, Maddalena DM, Makana J, Malhi Y, Marthews T, Mat Serudin R, McMahon SM, McShea WJ, Memiaghe HR, Mi X, Mizuno T, Morecroft M, Myers JA, Novotny V, de Oliveira AA, Ong PS, Orwig DA, Ostertag R, den Ouden J, Parker GG, Phillips RP, Sack L, Sainge MN, Sang W, Sri-Ngernyuang K, Sukumar R, Sun I, Sungpalee W, Suresh HS, Tan S, Thomas SC, Thomas DW, Thompson J, Turner BL, Uriarte M, Valencia R, Vallejo MI, Vicentini A, Vrška T, Wang X, Wang X, Weiblen G, Wolf A, Xu H, Yap S, Zimmerman J (2015) CTFS-ForestGEO: a worldwide network monitoring forests in an era of global change. Glob Change Biol 21:528–549

Barth MAF, Larson AJ, Lutz JA (2015) A forest reconstruction model to assess changes to Sierra Nevada mixed-conifer forest during the fire suppression era. For Ecol Manag 354:104–118

Belote RT, Larson AJ, Dietz MS (2015) Tree survival scales to community-level effects following mixed-severity fire in a mixed-conifer forest. For Ecol Manag 353:221–231

Blomdahl EM, Kolden CA, Meddens AJH, Lutz JA (2019) The importance of small fire refugia in the central Sierra Nevada, California, USA. For Ecol Manag 432:1041–1052

Boyden S, Montgomery R, Reich PB, Palik B (2012) Seeing the forest for the heterogeneous trees: stand-scale resource distributions emerge from tree-scale structure. Ecol Appl 22:1578–1588

Breece CR, Kolb TE, Dickson BG, McMillin JD, Clancy KM (2008) Prescribed fire effects on bark beetle activity and tree mortality in southwestern ponderosa pine forests. For Ecol Manag 255:119–128

Cansler CA, Swanson ME, Furniss TJ, Larson AJ, Lutz JA (2019) Fuel dynamics after reintroduced fire in an old-growth Sierra Nevada mixed-conifer forest. Fire Ecol 15:16

Cayan DR, Maurer EP, Dettinger MD et al (2008) Climate change scenarios for the California region. Clim Change 87:21–42

Churchill DJ, Carnwath GC, Larson AJ, Jeronimo SMA (2017) Historical forest structure, composition, and spatial pattern in dry conifer forests of the Western Blue Mountains, Oregon. General Technical Report PNW-GTR-956. USDA Forest Service Pacific Northwest Research Station, Portland

Churchill DJ, Larson AJ, Dahlgreen MC, Franklin JF, Hessburg PF, Lutz JA (2013) Restoring forest resilience: from reference spatial patterns to silvicultural prescriptions and monitoring. For Ecol Manag 291:442–457

Clyatt KA, Crotteau JS, Schaedel MS, Wiggins HL, Kelly H, Churchill DC, Larson AJ (2016) Historical spatial patterns and contemporary tree mortality in dry mixed-conifer forests. For Ecol Manag 361:23–37

Collins BM (2014) Fire weather and large fire potential in the northern Sierra Nevada. Agric For Meteorol 189–190:30–35

Das A, Battles J, van Mantgem PJ, Stephenson NL (2008) Spatial elements of mortality risk in old-growth forests. Ecology 89:1744–1756

Erdody TL, Moskal LM (2010) Fusion of LiDAR and imagery for estimating forest canopy fuels. Remote Sens Environ 114:725–737

Falk DA, Heyerdahl EK, Brown PM, Farris C, Fulé PZ, McKenzie D, Swetnam TW, Taylor AH, Van Horne ML (2011) Multi-scale controls of historical forest-fire regimes: new insights from fire-scar networks. Front Ecol Environ 9:446–454

Falk DA, Miller C, McKenzie D, Black AE (2007) Cross-scale analysis of fire regimes. Ecosystems 10:809–823

Fettig CJ, McKelvey SR, Cluck DR, Smith SL, Otrosina WJ (2010) Effects of prescribed fire and season of burn on direct and indirect levels of tree mortality in ponderosa and Jeffrey pine forests in California, USA. For Ecol Manag 260:207–218

Filip GM, Schmitt CL, Scott DW, Fitzgerald SA (2007) Understanding and defining mortality in western conifer forests. West J Appl For 22:105–115

Flint LE, Flint AL, Thorne JH, Boynton R (2014) 2014 California BCM (Basin Characterization Model) Downscaled Climate and Hydrology—30-year Summaries. California Climate Commons

Fulé PZ, Covington WW (1998) Spatial patterns of Mexican pine-oak forests under different recent fire regimes. Plant Ecol 134:197–209

Furniss TJ, Larson AJ, Kane VR, Lutz JA (2019) Multi-scale assessment of post-fire tree mortality models. Int J Wildland Fire 28:46–61

Gelfand AE, Ghosh SK (1998) Model choice: a minimum posterior predictive loss approach. Biometrika 85:1–11

Gelman A, Carlin JB, Stern HS, Rubin DB (2004) Bayesian data analysis. Texts in statistical science series. Chapman and Hall/CRC, Boca Raton

Gelman A, Hwang J, Vehtari A (2014) Understanding predictive information criteria for Bayesian models. Stat Comput 24:997–1016

Gelman A, Rubin DB (1992) Inference from iterative simulation using multiple sequences. Stat Sci 457–472

George EI, McCulloch RE (1993) Variable selection via Gibbs sampling. J Am Stat Assoc 88:881–889

Gersonde RF, O'Hara KL (2005) Comparative tree growth efficiency in Sierra Nevada mixed-conifer forests. For Ecol Manag 219:95–108

Gill L, Taylor AH (2009) Top-down and bottom-up controls on fire regimes along an elevational gradient on the east slope of the Sierra Nevada, California, USA. Fire Ecol 5:57–75

Guarín A, Taylor AH (2005) Drought triggered tree mortality in mixed conifer forests in Yosemite National Park, California, USA. For Ecol Manag 218:229–244

Hessburg PF, Agee JK, Franklin JF (2005) Dry forests and wildland fires of the inland Northwest USA: contrasting the landscape ecology of the pre-settlement and modern eras. For Ecol Manag 211:117–139

Hessburg PF, Churchill DJ, Larson AJ, Haugo RD, Miller C, Spies TA, North MP, Povak NA, Belote RT, Singleton PH, Gaines WL (2015) Restoring fire-prone Inland Pacific landscapes: seven core principles. Landsc Ecol 30:1805–1835

Heyerdahl EK, Brubaker LB, Agee JK (2001) Spatial controls of historical fire regimes: a multiscale example from the interior west, USA. Ecology 82:660–678

Hood SM (2010) Mitigating old tree mortality in long-unburned, fire-dependent forests: a synthesis. General Technical Report RMRS-GTR-238. USDA Forest Service Rocky Mountain Research Station, Fort Collins

Hood S, Bentz B (2007) Predicting postfire Douglas-fir beetle attacks and tree mortality in the northern Rocky Mountains. Can J For Res 37:1058–1069

Hood SM, McHugh CW, Ryan KC, Reinhardt E, Smith SL (2007) Evaluation of a post-fire tree mortality model for western USA conifers. Int J Wildland Fire 16:679–689

Hood SM, Smith SL, Cluck DR (2010) Predicting mortality for five California conifers following wildfire. For Ecol Manag 260:750–762

Hood SM, Varner JM, van Mantgem P, Cansler CA (2018) Fire and tree death: understanding and improving modeling of fire-induced tree mortality. Environ Res Lett 13:113004

Jakubowski MK, Guo Q, Kelly M (2013) Tradeoffs between lidar pulse density and forest measurement accuracy. Remote Sens Environ 130:245–253

Jenkins MJ, Runyon JB, Fettig CJ, Page WG, Bentz BJ (2014) Interactions among the mountain pine beetle, fires, and fuels. For Sci 60:489–501

Jeronimo SMA, Kane VR, Churchill DJ, McGaughey RJ, Franklin JF (2018) Applying LiDAR individual tree

detection to management of structurally diverse forest landscapes. J For 116:336–346
Jeronimo SMA, Kane VR, Churchill DJ, Lutz JA, North MP, Asner GP, Franklin JF (2019) Forest structure and pattern vary by climate and landform across active-fire landscapes in the montane Sierra Nevada. For Ecol Manag. https://doi.org/10.1016/j.foreco.2019.01.033
Kane VR, Bakker JD, McGaughey RJ, Lutz JA, Gersonde RF, Franklin JF (2010) Examining conifer canopy structural complexity across forest ages and elevations with LiDAR data. Can J For Res 40:774–787
Kane VR, Bartl-Geller BN, North MP, Kane JT, Lydersen JM, Jeronimo SMA, Collins BM, Moskal LM (2019) First-entry wildfires can create opening and tree clump patterns characteristic of resilient forests. For Ecol Manag 454:117659
Kane VR, Cansler CA, Povak NA, Kane JT, McGaughey RJ, Lutz JA, Churchill DJ, North MP (2015a) Mixed severity fire effects within the Rim Fire: relative importance of local climate, fire weather, topography, and forest structure. For Ecol Manag 358:62–79
Kane VR, Lutz JA, Cansler CA, Povak NA, Churchill DJ, Smith DF, Kane JT, North MP (2015b) Water balance and topography predict fire and forest structure patterns. For Ecol Manag 338:1–13
Kane VR, Lutz JA, Roberts SL, Smith DF, McGaughey RJ, Povak NA, Brooks ML (2013) Landscape-scale effects of fire severity on mixed-conifer and red fir forest structure in Yosemite National Park. For Ecol Manag 287:17–31
Kane VR, North MP, Lutz JA, Churchill DJ, Roberts SL, Smith DF, McGaughey RJ, Kane JT, Brooks ML (2014) Assessing fire effects on forest spatial structure using a fusion of Landsat and airborne LiDAR data in Yosemite National Park. Remote Sens Environ 151:89–101
Kennedy MC, Johnson MC (2014) Fuel treatment prescriptions alter spatial patterns of fire severity around the wildland–urban interface during the Wallow Fire, Arizona, USA. For Ecol Manag 318:122–132
Keyser TL, Smith FW, Lentile LB, Shepperd WD (2006) Modeling postfire mortality of ponderosa pine following a mixed-severity wildfire in the Black Hills: the role of tree morphology and direct fire effects. For Sci 52:530–539
Kolden CA, Lutz JA, Key CH et al (2012) Mapped versus actual burned area within wildfire perimeters: characterizing the unburned. For Ecol Manag 286:38–47
Kotliar NB, Wiens JA (1990) Multiple scales of patchiness and patch structure: a hierarchical framework for the study of heterogeneity. Oikos 253–260
Kramer H, Collins B, Kelly M, Stephens S (2014) Quantifying ladder fuels: a new approach using LiDAR. Forests 5:1432–1453
Kramer H, Collins B, Lake F et al (2016) Estimating ladder fuels: a new approach combining field photography with LiDAR. Remote Sens 8:766
Larson AJ, Churchill DJ (2012) Tree spatial patterns in fire-frequent forests of western North America, including mechanisms of pattern formation and implications for designing fuel reduction and restoration treatments. For Ecol Manag 267:74–92
Lusk CH (2002) Leaf area accumulation helps juvenile evergreen trees tolerate shade in a temperate rainforest. Oecologia 132:188–196
Lutz JA (2015) The evolution of long-term data for forestry: large temperate research plots in an era of global change. Northwest Sci 89:255–269
Lutz JA, Furniss TJ, Germain SJ et al (2017) Shrub communities, spatial patterns, and shrub-mediated tree mortality following reintroduced fire in Yosemite National Park, California, USA. Fire Ecol 13:104–126
Lutz JA, Furniss TJ, Johnson DJ et al (2018b) Global importance of large-diameter trees. Glob Ecol Biogeogr 27:849–864
Lutz JA, Larson AJ, Freund JA et al (2013) The importance of large-diameter trees to forest structural heterogeneity. PLoS ONE 8:e82784
Lutz J, Larson A, Swanson M (2018a) Advancing fire science with large forest plots and a long-term multidisciplinary approach. Fire 1:5
Lutz JA, Larson AJ, Swanson ME, Freund JA (2012) Ecological importance of large-diameter trees in a temperate mixed-conifer forest. PLoS ONE 7:e36131
Lutz JA, Van Wagtendonk JW, Franklin JF (2009a) Twentieth-century decline of large-diameter trees in Yosemite National Park, California, USA. For Ecol Manag 257:2296–2307
Lutz JA, van Wagtendonk JW, Franklin JF (2010) Climatic water deficit, tree species ranges, and climate change in Yosemite National Park. J Biogeogr 37:936–950
Lutz JA, Van Wagtendonk JW, Thode AE, Miller JD, Franklin JF (2009b) Climate, lightning ignitions, and fire severity in Yosemite National Park, California, USA. Int J Wildland Fire 18:765–774
Lydersen JM, Collins BM, Brooks ML, Matchett JR, Shive KL, Povak NA, Kane VR, Smith DF (2017) Evidence of fuels management and fire weather influencing fire severity in an extreme fire event. Ecol Appl 27:2013–2030
Lydersen JM, North MP, Collins BM (2014) Severity of an uncharacteristically large wildfire, the Rim Fire, in forests with relatively restored frequent fire regimes. For Ecol Manag 328:326–334
Maher CT, Oja E, Marshall A et al (2019) Real-time monitoring with a tablet App improves implementation of treatments to enhance forest structural diversity. J For 117:280–292
McKenzie D, Kennedy MC (2011) Scaling laws and complexity in fire regimes. The landscape ecology of fire. Springer, Dordrecht, pp 27–49
Meddens AJH, Kolden CA, Lutz JA et al (2018) Fire refugia: what are they and why do they matter for global change? Bioscience 68:944–954
Merschel AG, Heyerdahl EK, Spies TA, Loehman RA (2018) Influence of landscape structure, topography, and forest type on spatial variation in historical fire regimes, Central Oregon, USA. Landsc Ecol 33:1195–1209
Miller JD, Safford HD, Welch KR (2016) Using one year post-fire fire severity assessments to estimate longer-term effects of fire in conifer forests of northern and eastern California, USA. For Ecol Manag 382:168–183
Miller C, Urban DL (1999) A model of surface fire, climate and forest pattern in the Sierra Nevada, California. Ecol Model 114:113–135

North M, Stine P, O'Hara K et al (2009) An ecosystem management strategy for Sierran mixed-conifer forests. General Technical Report PSW-GTR-220. USDA Forest Service Pacific Southwest Research Station, Albany

O'Brien JJ, Kevin Hiers J, Mitchell RJ et al (2010) Acute physiological stress and mortality following fire in a long-unburned longleaf pine ecosystem. Fire Ecol 6:1–12

Palik BJ, Goebel PC, Kirkman LK, West L (2000) Using landscape hierarchies to guide restoration of disturbed ecosystems. Ecol Appl 10:189–202

Parks SA, Holsinger LM, Miller C, Nelson CR (2015) Wildland fire as a self-regulating mechanism: the role of previous burns and weather in limiting fire progression. Ecol Appl 25:1478–1492

Parks SA, Parisien M-A, Miller C (2012) Spatial bottom-up controls on fire likelihood vary across western North America. Ecosphere 3:1–20

Parsons AR, Linn RR, Pimont F et al (2017) Numerical investigation of aggregated fuel spatial pattern impacts on fire behavior. Land 6(2):43

Parsons R, Jolly WM, Hoffman C, Ottmar R (2016) The role of fuels in extreme fire behavior. In: Synthesis of knowledge of extreme fire behavior, p 55

Parsons RA, Pimont F, Wells L, Cohn G, Jolly WM, de Coligny F, Rigolot E, Dupuy JL, Mell W, Linn RR (2018) Modeling thinning effects on fire behavior with STANDFIRE. Ann For Sci 75:7

Plummer M (2003) JAGS: a program for analysis of Bayesian graphical models using Gibbs sampling. In: Proceedings of the 3rd international workshop on distributed statistical computing, Vienna, Austria

Plummer M (2016a) JAGS-4.2.0

Plummer M (2016b) rjags: Bayesian Graphical Models using MCMC

Prichard SJ, Kennedy MC (2012) Fuel treatment effects on tree mortality following wildfire in dry mixed conifer forests, Washington State, USA. Int J Wildland Fire 21:1004–1013

R Core Team (2016) R: a language and environment for statistical computing. R Foundation for Statistical Computing, Vienna

Richardson JJ, Moskal LM, Kim S-H (2009) Modeling approaches to estimate effective leaf area index from aerial discrete-return LIDAR. Agric For Meteorol 149:1152–1160

Ryan KC, Reinhardt ED (1988) Predicting postfire mortality of seven western conifers. Can J For Res 18:1291–1297

Salomón RL, Tarroux E, DesRochers A (2016) Natural root grafting in *Picea mariana* to cope with spruce budworm outbreaks. Can J For Res 46:1059–1066

Simard SW (2009) The foundational role of mycorrhizal networks in self-organization of interior Douglas-fir forests. For Ecol Manag 258:S95–S107

Smith AMS, Sparks AM, Kolden CA et al (2016) Towards a new paradigm in fire severity research using dose–response experiments. Int J Wildland Fire 25:158–166

Stephens SL (1998) Evaluation of the effects of silvicultural and fuels treatments on potential fire behaviour in Sierra Nevada mixed-conifer forests. For Ecol Manag 105:21–35

Stephens SL, Collins BM, Fettig CJ et al (2018) Drought, tree mortality, and wildfire in forests adapted to frequent fire. Bioscience 68:77–88

Stephens SL, Fry DL (2005) Spatial distribution of regeneration patches in an old-growth *Pinus jeffreyi*-mixed conifer forest in northwestern Mexico. J Veg Sci 16:693–702

Stephens SL, Moghaddas JJ (2005) Silvicultural and reserve impacts on potential fire behavior and forest conservation: twenty-five years of experience from Sierra Nevada mixed conifer forests. Biol Conserv 125:369–379

USDA (2016) FireFamilyPlus, 4.2. https://www.firelab.org/document/firefamilyplus-software. Accessed 1/12/2017

van Mantgem PJ, Falk DA, Williams EC et al (2018) Pre-fire drought and competition mediate post-fire conifer mortality in western US National Parks. Ecol Appl 28:1730–1739

van Mantgem PJ, Nesmith JCB, Keifer M et al (2013) Climatic stress increases forest fire severity across the western United States. Ecol Lett 16:1151–1156

Van Mantgem PJ, Stephenson NL, Knapp E et al (2011) Long-term effects of prescribed fire on mixed conifer forest structure in the Sierra Nevada, California. For Ecol Manag 261:989–994

Warren JM, Brooks JR, Meinzer FC, Eberhart JL (2008) Hydraulic redistribution of water from *Pinus ponderosa* trees to seedlings: evidence for an ectomycorrhizal pathway. N Phytol 178:382–394

Weiss A (2001) Topographic position and landforms analysis. In: Poster presentation, ESRI user conference, San Diego, CA

Wiggins HL, Nelson CR, Larson AJ, Safford HD (2019) Using LiDAR to develop high-resolution reference models of forest structure and spatial pattern. For Ecol Manag 434:318–330

Williams AP, Seager R, Macalady AK et al (2015) Correlations between components of the water balance and burned area reveal new insights for predicting forest fire area in the southwest United States. Int J Wildland Fire 24:14–26

Woolley T, Shaw DC, Ganio LM, Fitzgerald S (2012) A review of logistic regression models used to predict post-fire tree mortality of western North American conifers. Int J Wildland Fire 21:1–35

Young DJN, Stevens JT, Earles JM et al (2017) Long-term climate and competition explain forest mortality patterns under extreme drought. Ecol Lett 20:78–86

Youngblood A, Grace JB, McIver JD (2009) Delayed conifer mortality after fuel reduction treatments: interactive effects of fuel, fire intensity, and bark beetles. Ecol Appl 19:321–337